



ELSEVIER

Contents lists available at ScienceDirect

Journal of Magnetism and Magnetic Materials

journal homepage: www.elsevier.com/locate/jmmm

Detection of molecules and cells using nuclear magnetic resonance with magnetic nanoparticles

Christine Rümenapp^{a,*}, Bernhard Gleich^a, Hans Georg Mannherz^b, Axel Haase^a^a Zentralinstitut für Medizintechnik (IMETUM), Technische Universität München, Garching, Germany^b Abteilung für Anatomie und Molekulare Embryologie, Ruhr Universität Bochum, Bochum, Germany

ARTICLE INFO

Article history:

Received 30 June 2014

Received in revised form

22 August 2014

Accepted 2 September 2014

Available online 10 September 2014

Keywords:

Magnetic nanoparticles

Co-precipitation

Nuclear magnetic resonance

 T_2 relaxation time

Detection

Particle clustering

ABSTRACT

For the detection of small molecules, proteins or even cells *in vitro*, functionalised magnetic nanoparticles and nuclear magnetic resonance measurements can be applied. In this work, magnetic nanoparticles with the size of 5–7 nm were functionalised with antibodies to detect two model systems of different sizes, the protein avidin and *Saccharomyces cerevisiae* as the model organism. The synthesised magnetic nanoparticles showed a narrow size distribution, which was determined using transmission electron microscopy and dynamic light scattering. The magnetic nanoparticles were functionalised with the according antibodies via EDC/NHS chemistry. The binding of the antigen to magnetic nanoparticles was detected through the change in the NMR T_2 relaxation time at 0.5 T (≈ 21.7 MHz). In case of a specific binding the particles cluster and the T_2 relaxation time of the sample changes. The detection limit in buffer for FITC-avidin was determined to be 1.35 nM and 10^7 cells/ml for *S. cerevisiae*. For fluorescent microscopy the avidin molecules were labelled with FITC and for the detection of *S. cerevisiae* the magnetic nanoparticles were additionally functionalised with rhodamine. The binding of the particles to *S. cerevisiae* and the resulting clustering was also seen by transmission electron microscopy.

© 2014 Elsevier B.V. All rights reserved.

1. Introduction

Magnetic nanoparticles (MNPs) can be monodisperse, superparamagnetic, nanometer-sized particles and made of iron oxides. The first commercial particles with biocompatible coatings, like dextran, silica or carboxylates were contrast agents for magnetic resonance imaging (MRI) [1–4]. MNPs, which are binding specifically to a target, can also be used for purification and separation techniques as well as for magnetic transfection of cultured cells [5–8]. These particles are larger than 10 nm or even in the micrometer size range making it easier to trap them with magnetic fields due to their higher magnetic moments [9].

Combining the purification method and MRI, the nuclear magnetic resonance (NMR) T_2 relaxation time of the sample changes, if the MNPs bind to a target and agglomerate. Roch et al. examined the theory of the changes of the proton relaxation times in the presence of MNPs in more detail [10]. By the use of theoretical models, they showed a dependence of the NMR T_2 relaxation time on the MNP size [11,12]. For superparamagnetic nanoparticles this theory is called the outer sphere relaxation theory [13–16]. Depending on the size of MNPs they belong to different regimes, in which the NMR T_2

relaxation time of the sample is influenced in different ways. Very small particles (< 20 nm) belong to the motional averaging regime, where the NMR T_2 relaxation time decreases as the size of the particle core or the cluster increases. A further size increase to the size range of 20 to 100 nm, makes the particles part of the slow motion regime. Here, the NMR T_2 relaxation time stays in the same range. Most of the used contrast agents are in this size regime. For even larger sizes the particles are part of the echo limited regime and the NMR T_2 relaxation time is increasing with the size of the particles core or the induced cluster. If MNPs cluster, the NMR T_2 relaxation time changes according to outer sphere relaxation theory. This change is caused by the difference in the field inhomogeneities between the colloidal state and the clustered state of the MNPs [17]. First applications of this effect were reported by Haun et al. who used the effect of the change in the T_2 relaxation time upon the clustering or dispersion of MNPs to detect small molecules, DNA, proteins, bacteria, viruses and cells [18]. Tumour tissue was also profiled with this technique for certain tumour markers [19]. The same effect is used for the new imaging modality of functional magnetic resonance imaging. Using this imaging technique it is possible to investigate for instance molecular pathways occurring in the brain upon learning [20].

So far, the detection of molecules and cells has been investigated using different sizes of particles and different functional moieties or ligands for the specific binding to the magnetic nanoparticles. We investigated the use of very small MNPs (core diameter 5–7 nm) with

* Corresponding author. Tel: +49 89 289 10816.

E-mail address: ruemenapp@tum.de (C. Rümenapp).

an antibody functionalisation for the detection of two model systems of different sizes. First, avidin was used as the reference protein (67 kDa) and secondly *Saccharomyces cerevisiae* yeast cells as the reference organism (2.5–5 μm).

2. Materials and methods

2.1. Materials

FeCl_2 tetrahydrate, 37% hydrochloric acid, NaOH pellets, $\text{Na}_2\text{B}_4\text{O}_7(\text{H}_2\text{O})_{10}$, dimethylsulfoxide (DMSO) and boric acid were purchased (Merck Chemicals) and used without further purification. 45% FeCl_3 hexahydrate solution was purchased from Riedel-deHaen and 69% nitric acid from Applichem. Bovine serum albumin (BSA) (BioZym), *N*-(3-dimethyl-aminopropyl)-*N'*-ethylcarbodiimide hydrochloride (EDC), *N*-hydroxysuccinimide (NHS), tetraethoxysilane (TEOS), (3-aminopropyl)-triethoxysilane (APTES) and Na_2HPO_4 were purchased (Sigma-Aldrich) and used without further purification. Antibodies were purchased from <http://www.antibodies-online.de> and the host was in both cases rabbit (anti-avidin antibody: ABIN116964; anti-*S. cerevisiae* antibody: ABIN260785).

2.2. Magnetic nanoparticle synthesis

For the synthesis of magnetic nanoparticles with a narrow size distribution the protocol from Forge et al. was applied with minor modifications as follows [21]. 45 mmol FeCl_2 tetrahydrate were dissolved in 37 mmol 45% FeCl_3 hexahydrate solution. 300 ml of diethylene glycol (DEG) were added under stirring with 150 rpm. The solution was purged with nitrogen throughout the reaction and was heated to 170 °C. Subsequently, 15 g of NaOH-pellets were quickly added. The suspension turned black immediately and was kept at 170 °C for 1 h. After returning to room temperature the particles were magnetically separated for 2.5 h. The peptisation of the particles was done by the method of Massart [22]. Briefly, the obtained particles were redispersed in 1 M HNO_3 using a magnetic stirrer. This washing step was repeated four times. After the last separation the particles were resuspended in $\text{H}_2\text{O}_{\text{dd}}$ at room temperature overnight. Subsequently, they were sonicated in a water bath at room temperature for 45 min and afterwards centrifuged at 16,700 rcf at 21 °C for 1 h. The supernatant containing the MNPs was carefully removed. The iron content of the particle suspensions was determined using the Fe Spectroquant Kit from Merck Chemicals.

2.3. Coating of magnetic nanoparticles

The first coating layer made of silica was applied by the condensation of TEOS. Briefly, to 20 ml particle suspension 40 ml $\text{H}_2\text{O}_{\text{dd}}$ were added and the mixture was heated to 50 °C under nitrogen flush and stirring. After equilibration, twice the amount of TEOS compared to the iron content of the suspension was dissolved in 10 ml 96% EtOH and added drop wise. The reaction was carried out at 50 °C under nitrogen atmosphere for 24 h. After homogenization in a sonication bath for 45 min the particles coated with TEOS (MNP-TEOS) were washed with $\text{H}_2\text{O}_{\text{dd}}$ using an ultrafiltration device with a cut-off of 30 kDa (Amicon, 8200 cell, Millipore). The concentrated MNP-TEOS were centrifuged at 4500 rcf at 21 °C for 45 min. The particles were aminated by the second layer with APTES for the covalent coupling of proteinaceous binding moieties. To 15 ml of MNP-TEOS 30 ml $\text{H}_2\text{O}_{\text{dd}}$ were added. To this suspension 1 ml of 1 M HNO_3 and APTES with 0.8 times the amount of the iron content of the MNP-TEOS solution were added. The reaction was heated to 70 °C

under nitrogen flush and stirring and incubated at this temperature for 2 h. The obtained MNP-APTES were washed and purified like MNP-TEOS.

2.4. Functionalisation of magnetic nanoparticles

Functionalisation with antibodies against FITC-avidin or *S. cerevisiae* was carried out using the EDC/NHS activation of the carboxy-groups on the surface of the antibody. To 300 μl anti-avidin antibody (10 mg/ml) 33.61 μl of NHS (10 mg/ml) and 89.56 μl of EDC (5 mg/ml) were added. NHS was dissolved in dimethylsulfoxide (DMSO) and EDC in 50 mM sodium borate buffer (50 mM boric acid, 50 mM sodium tetraborate, pH 8.17) directly before starting the reaction to prevent early hydrolysis. After incubation in a shaker at room temperature for 10 min, 1565 μl of Fe MNP-APTES (229 mM) were added. The volume of the reaction was increased to 5 ml using a 50 mM sodium borate buffer, pH 8.17. The reaction was performed on a rotating wheel at room temperature for 2 h. Subsequently, ultrafiltration was performed with a 300 kDa cut-off and blocking buffer (10 mM Na_2HPO_4 , 1% BSA w/v, 0.01% NaN_3 w/v, pH 7.4) to remove un-reacted reagents and antibodies. The supernatant was removed and stored at 4 °C until further use. Functionalisation with an anti-*S. cerevisiae* antibody was performed in the same way with an antibody concentration of 1 mg/ml. To generate anti-*S. cerevisiae* rhodamine MNPs, 10 mmol NHS-rhodamine dissolved in 100 μl DMSO was added to 1 mmol antibody on the particles and incubated in the dark at room temperature for 1 h. The anti-*S. cerevisiae* rhodamine MNPs were washed via ultrafiltration with blocking buffer until the red colour of the eluate disappeared.

2.5. Electron microscopy of MNPs

Transmission electron microscopy (TEM) of MNPs, coated and functionalised MNPs was performed with a JEM100 CX at 100 kV. 5 μl of MNP suspensions with appropriate dilutions were applied to a 300 mesh grid coated with carbon for the naked MNPs or to a 300 mesh grid coated with a holey carbon film (2 nm thickness) for the coated MNPs and antibody MNPs. Subsequently, the particles were air-dried at room temperature. Antibody-MNPs were contrasted with 2% (w/v) uranyl acetate following standard procedures.

2.6. Electron microscopy of yeast cells after incubation with MNPs

Yeast cells were incubated with or without nanoparticles for 24 h and thereafter fixed with 2% glutaraldehyde dissolved in PBS for 2 days. After centrifugation the cell pellets were treated with 2% (w/v) osmium tetroxide, transferred to gelatin tubes, and Epon embedded following standard procedures. Sections of 300 to 500 nm thickness were prepared with a Leitz ultramicrotome and examined in a Philips 420 electron microscope operated at 80 kV.

2.7. Size characterisation

Size determination was done using TEM and dynamic light scattering (DLS). The size distribution of the MNP cores was determined from TEM images with the image-processing software *ImageJ* with the feature *Analyze Particles*. The hydrodynamic diameter of the particles at all stages of synthesis with a concentration of 10 mM Fe was determined with the Zetasizer Nanoseries NanoZS from Malvern Instruments.

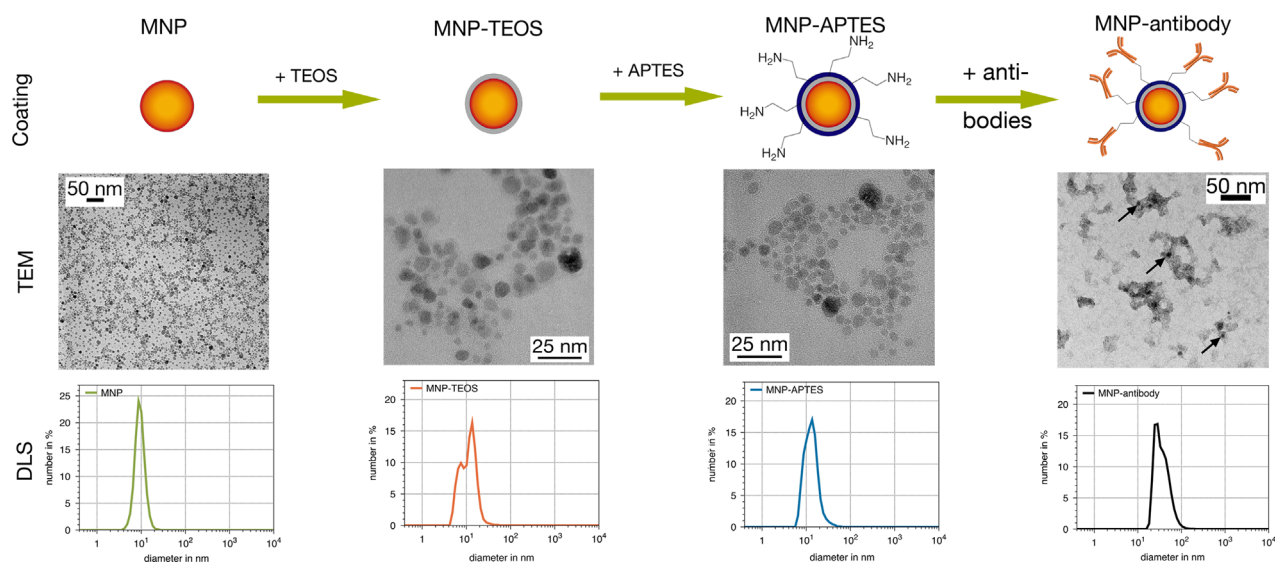


Fig. 1. Size determination with DLS measurements with a number distribution for the MNPs and the according TEM images. The core of the MNPs had a diameter of 5.8 ± 1.7 nm in TEM analysis and 9.7 ± 1.1 nm in DLS. MNP-TEOS were 11.8 ± 4.1 nm and MNP-APTES 13.7 ± 3.6 nm in hydrodynamic diameter. The antibody-MNPs had a hydrodynamic diameter of 30.14 ± 13.08 nm. As an example the TEM image of anti-avidin MNPs is presented. Arrows indicate MNPs.

2.8. NMR T_2 relaxation time measurements

NMR measurements were performed at room temperature and 0.5 T (≈ 21.7 MHz) using the Research Lab device from Pure Devices. Each NMR T_2 relaxation time was determined using the Carr–Purcell–Meiboom–Gill (CPMG) pulse sequence with an echo time of 3 ms. Measurements for anti-avidin MNPs were conducted with different concentrations of avidin and streptavidin as negative control after an incubation of 15 min. For anti-*S. cerevisiae* MNPs the measurements were conducted with different concentrations of *S. cerevisiae* cells. The iron content was kept at 0.22 mM Fe and all measurements were done in phosphate buffered saline (PBS), pH 7.4, in triplets.

3. Results

3.1. Dynamic light scattering and transmission electron microscopy

The mean diameter of the particle core obtained by TEM image analysis was 5.8 ± 1.7 nm determination by DLS gave 9.7 ± 1.1 nm in number distribution (Fig. 1). The increase of the particle diameter with every coating was documented by DLS. For the MNP-TEOS the mean diameter in number distribution increased to 11.8 ± 4.1 nm and for the MNP-APTES to 13.7 ± 3.6 nm (Fig. 1). The functionalisation with antibodies leads to a final diameter in number distribution of 30.14 ± 13.08 nm. The poly-dispersity index (Pdl) as reference for the monodispersity of the samples was in all cases between 0.24 and 0.26. The applied coating and the functionalisation with antibodies can be seen clearly in the TEM images (Fig. 1).

3.2. Relaxation time measurements

As can be seen in Fig. 2a and Fig. 3a, the clustering of the particles changed their NMR T_2 relaxation time. For FITC-avidin this change was more than 40% of the initial value of the NMR T_2 relaxation time. The lowest concentration of FITC-avidin, which was detectable with a change of more than 25% of the T_2 relaxation time, was 1.35 nM (Fig. 2a). The clustering of the MNPs due to the binding of FITC-avidin was confirmed with fluorescent microscopy (Fig. 2b). The negative control was performed with

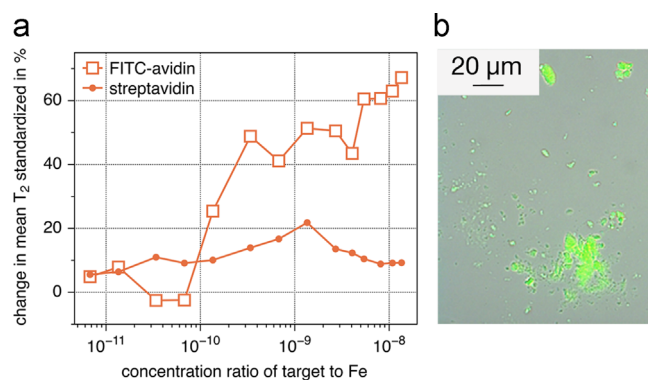


Fig. 2. Changes of the NMR T_2 relaxation time due to the binding of anti-avidin MNPs to different concentrations of FITC-avidin and streptavidin as control (a). The clustering of the anti-avidin MNPs leads to an increase in the NMR T_2 relaxation time, which was also seen in fluorescent microscopic images for FITC-avidin (b). The detection limit for FITC-avidin in PBS was 1.35 nM.

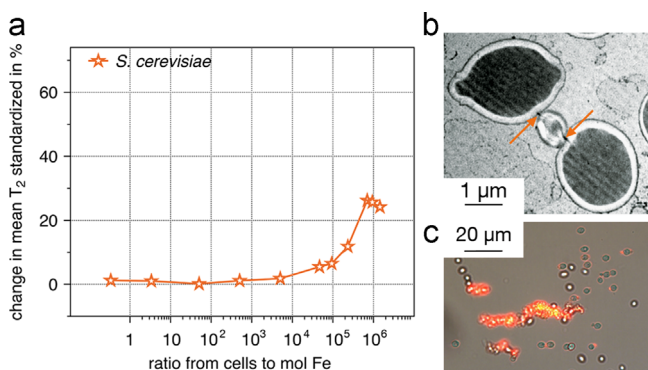


Fig. 3. Changes of the NMR T_2 relaxation time due to the binding of anti-*S. cerevisiae* MNPs to *S. cerevisiae* in different concentrations (a). The detection limit for *S. cerevisiae* in PBS was 10^7 cells/ml. The binding of the particles to *S. cerevisiae* and the resulting clustering was seen in TEM images (b) and by fluorescent microscopy after the particles were additionally functionalised with rhodamine (c).

streptavidin. The antibodies used are specific for avidin, which was confirmed by Western blot (data not shown). Streptavidin was used in the same concentrations as avidin. However, the change of

the T_2 relaxation time first increases to around 20% of the initial value to decrease again (Fig. 2a). In contrast to the measurements with avidin, the change in the T_2 relaxation time did not increase further or stayed at the same level once it was increased like it would be expected for a dose-response curve. There was also no clustering of the MNPs seen under the microscope. For the detection of *S. cerevisiae* the change in the T_2 relaxation time increases to over 25% and stayed in this range (Fig. 3a). This change in T_2 relaxation time corresponds to a concentration of *S. cerevisiae* of 10^7 cells/ml. The clustering of the MNPs was seen with TEM (Fig. 3b) and via fluorescent microscopy (Fig. 3c) confirming the binding of the MNPs to the *S. cerevisiae*.

4. Discussion

In TEM image analysis, the diameter of each single particle is measured and morphological information is provided at the same time. Using DLS measurements the hydrodynamic diameter can be obtained very quickly in a few minutes. The measurements are done in the liquid environment of the samples and represent large ensembles of the particles and not just a few. However, the size for the particle core obtained by DLS measurements is larger compared to the size obtained by TEM image analysis. Since the naked particles are strongly charged due to the peptisation treatment, they are surrounded by a hydration layer, which is bound very tightly. Furthermore, in DLS measurements larger particles are always more prominent in their detection than smaller particles, shifting the obtained diameter to larger values [23]. To determine the differences in diameters of mono-disperse suspensions, DLS measurements can be considered reliable. The particles are coated with a thin layer of approximately 2 nm thickness and their diameter is increased by 16.5 nm due to the antibody functionalisation with the antibodies being approximately 7 nm long [24]. When applying NMR T_2 relaxation time measurements, a thin coating is preferable for the measurement of the outer sphere relaxation of the protons. If the coating were too thick, the steric hindrance of the water protons would be too large for them to come close enough to the induced magnetic field of the particles. Therefore they would not be influenced in their relaxation. Thus, a thin coating improves the signal change in the NMR T_2 relaxation time detection measurements.

The detection in complex matrices like serum, plasma or blood samples involve many unpredictable influences, which need to be considered. We therefore, chose simple aqueous matrices like buffer solutions for the detection of small molecules, proteins and cells *in vitro*.

The detection of avidin with anti-avidin MNPs was successful already at a concentration as low as 1.35 nM. This is half the concentration of avidin, which was detected so far by using biotin as the binding ligand. In this case, avidin has been detected using MNPs with a core diameter of 7 nm and a functionalisation with biotin leading to hydrodynamic diameter of 38 nm at a magnetic flux density of 0.47 T [25]. At a concentration of 0.2 mM Fe, 5.83 nM avidin was detected, which is twice the concentration we detected with our antibody functionalised particles. The better performance of the synthesised MNPs could be due to their smaller coating layer leading to a better influence of the outer sphere relaxation of the water protons. It has to be mentioned that due to different measurements set-ups in the former measurements the volume was 2 μ l, whereas in our case it was 200 μ l.

In contrast, the detection limit of 10^7 cells/ml is still high. For larger targets the particles still need to be modified to reach a better detection limit. In the literature *Staphylococcus aureus* has been detected using the same method at a concentration as low as 5×10^3 bacteria/ml [25]. The used MNP were functionalised with

vancomycin and had a core diameter of 7 nm and a hydrodynamic diameter with coatings of 38 nm. This detection limit is five magnitudes, i.e. 10^5 fold lower compared to the obtained detection limit for *S. cerevisiae*. There are several possible reasons for this. One reason is the different size of the target organism. The yeast cells are between 2.5 and 5 μ m in diameter, whereas the bacteria are about 1 μ m in size. However, using the same system, mouse macrophages of 10 μ m were detected at a concentration of 100 cells/ml [26]. Another reason could be a low binding performance of the antibody. This can cause some MNP to be in-effective in binding and will lead to a reduced target to MNP ratio, since more anti-*S. cerevisiae* MNPs have to be used for the detection. Furthermore, the size of the MNP could be improved. Koh et al. showed that targets of large sizes with many valencies for the binding of a possible immobilized ligand show better detection thresholds, if they are detected with MNPs of μ m size range [27]. They compared MNPs with a diameter of 70 nm and MNPs with a diameter of 1 μ m for their detection performance of targets of different sizes (8 nm and 900 nm) additionally differing in their valencies. However, a direct comparison of their results with the yeast target of 2.5 μ m size and a MNP with a hydrodynamic diameter of 30 nm, as used in our study, is difficult. Nevertheless, they concluded that their largest target of 900 nm diameter was detected at a better threshold using the larger particles of 1 μ m in diameter. By using a 10 times larger MNP they decreased their detection limit of the large targets by a factor of 10^6 . Following these calculations a decrease of the detection limit to 10^2 cells/ml would result if a bigger core and therefore a bigger hydrodynamic radius and a greater magnetic moment would be used for the detection of *S. cerevisiae* yeast cells. Furthermore, by using an antibody with a higher binding affinity, MNP binding should be more effective and the probability of fully functional anti-*S. cerevisiae* MNPs would be higher. The larger particles would also lead to a larger surface with a higher density of antibodies per MNP. Therefore, it appears reasonable to predict that a higher affinity of the antibody to its target could lead to a detection limit as low as 1 cell/ml. This would be preferable for the future applications in, for example, quality control or pharmaceuticals. More detailed studies for this problem are under way.

5. Conclusion

MNPs need a thin coating to be colloiddally stable and thus to be appropriate for NMR T_2 relaxation time measurements. The applied coating was of 1.96 nm thickness as determined by DLS measurements leading to a final hydrodynamic diameter of 13.65 ± 3.64 nm. The further functionalisation of APTES coated MNPs was conducted by carbodiimide chemical cross-linking. The used antibodies were applied as a monolayer around the particles, which was determined by the hydrodynamic radius increase of 8.25 nm. The functionalisation method is fast, reliable and can be performed without using harmful chemicals. The first system to test the preparation protocol of the MNPs and the detection method was the avidin system. FITC-avidin was detected at a concentration of 1.35 nM in PBS. This detection level was twofold higher than the detection levels for avidin reported so far [25]. The second system was the application of the method for the detection of *S. cerevisiae*. Here a detection limit of 10^7 cells/ml in PBS was achieved using anti-*S. cerevisiae* MNPs. The successful binding of the MNPs to *S. cerevisiae* was verified by fluorescence and transmission electron microscopy. The detection limit is too high for an *in vitro* application and needs improvement. This may be achieved by preparing particles with a larger core size and therefore a larger magnetic moment leading for this particular target to

a better sensitivity in the NMR T_2 relaxation time measurements. Further experiments will include NMR relaxation measurements with MNPs of a larger core size and their functionalisation with an antibody of higher affinity.

Acknowledgements

The authors like to thank M. Hanzlik from the Technische Universität München for performing transmission electron microscopy of the MNPs, Prof. C. Theiss and Mrs. H.-T. Nguyen for help in embedding and sectioning the yeast cells, and S. Huber for the technical support.

References

- [1] C. Corot, et al., Recent advances in iron oxide nanocrystal technology for medical imaging, *Adv. Drug Delivery Rev.* 58 (2006) 1471–1504.
- [2] S. Laurent, et al., Magnetic iron oxide nanoparticles: synthesis, stabilization, vectorization, physicochemical characterizations, and biological applications, *Chem. Rev.* 108 (6) (2008) 2064–2110.
- [3] Q.A. Pankhurst, et al., Applications of magnetic nanoparticles in biomedicine, *J. Phys. D: Appl. Phys.* 36 (13) (2003) 167.
- [4] R. Stephen Zachary, M. Kievit Forrest, M. Zhang, Magnetite nanoparticles for medical MR imaging, *Mater. Today* 14 (2011) 330–338.
- [5] G. Fonnum, et al., Characterisation of Dynabeads by magnetization measurements and Mössbauer Spectroscopy, *J. Magn. Magn. Mater.* 293 (1) (2005) 41–47.
- [6] M. Heyd, M. Franzreb, S. Berensmeier, Integrierte Produktion und Separation von Biotensiden im Mehrphasenreaktor, *CIT* 82 (2010) 111–115.
- [7] J. Hu, G. Chen, I.M.C. Lo, Removal and recovery of Cr(VI) from wastewater by maghemite nanoparticles, *Water Res.* 39 (18) (2005) 4528–4536.
- [8] C. Plank, et al., The magnetofection method: using magnetic force to enhance gene delivery, *Biol. Chem.* 384 (2003) 737–747.
- [9] S. Mørup, M.F. Hansen, C. Frandsen, Magnetic nanoparticles, in: G.D. D.La.S. Andrews, G. P. Wiederrecht (Eds.), *Comprehensive Nanoscience and Technology*, Academic Press, Amsterdam, 2011, pp. 437–491.
- [10] A. Roch, N. M.R., P. Gillis, Theory of proton relaxation induced by superparamagnetic particles, *J. Chem. Phys.* 110 (1999) 5403–5411.
- [11] Q.L. Vuong, P. Gillis, Y. Gossuin, Monte Carlo simulation and theory of proton NMR transverse relaxation induced by aggregation of magnetic particles used as MRI contrast agents, *J. Magn. Reson.* 212 (1) (2011) 139–148.
- [12] A. Roch, et al., Water magnetic relaxation in superparamagnetic colloid suspensions: the effect of agglomeration, *Magnetic Resonance in Colloid and Interface Science*, Springer, Netherlands (2002) 383–392.
- [13] J.K. Kirsch, Basic principles of magnetic resonance contrast agents, *Top. Magn. Reson. Imaging* (1991) 13 (1991) 1.
- [14] Y. Gossuin, et al., Magnetic resonance relaxation properties of superparamagnetic particles, *Wiley Interdiscip. Rev. Nanomed. Nanobiotechnol.* 1 (3) (2009) 299–310.
- [15] P. Gillis, H.K.S., Transverse relaxation of solvent protons induced by magnetized spheres: application to ferritin, erythrocytes, and magnetite, *Magn. Reson. Med.* 5 (1987) 323–345.
- [16] P. Gillis, F. Moiny, R.A. Brooks, On T(2)-shortening by strongly magnetized spheres: a partial refocusing model, *Magn. Reson. Med.* 47 (2) (2002) 257–263.
- [17] C. Rügenapp, B. Gleich, A. Haase, Magnetic nanoparticles in magnetic resonance imaging and diagnostics, *Pharm. Res.* (2012) 1–15.
- [18] J.B. Haun, et al., Magnetic nanoparticle biosensors, *Wiley Interdiscip. Rev. Nanomed. Nanobiotechnol.* 2 (2010) 291–304.
- [19] H. Lee, et al., Rapid detection and profiling of cancer cells in fine-needle aspirates, *Proc. Natl. Acad. Sci. U.S.A.* 106 (30) (2009) 12459–12464.
- [20] G.G. Westmeyer, Y. Durocher, A. Jasanoff, A secreted enzyme reporter system for MRI, *Angew. Chem. Int. Ed. Engl.* 49 (23) (2010) 3909–3911.
- [21] D. Forge, et al., Optimization of the synthesis of superparamagnetic contrast agents by the design of experiments method, *J. Phys. Chem. C* 112 (49) (2008) 19178–19185.
- [22] R. Massart, Preparation of aqueous magnetic liquids in alkaline and acidic media, *IEEE Trans. Magn.* 17 (2) (1981) 1247–1248.
- [23] N.C. Bell, et al., Emerging Techniques for Submicrometer Particle Sizing Applied to Stöber Silica, *Langmuir* 28 (29) (2012) 10860–10872.
- [24] N. Ban, et al., Crystal structure of an idiotype-anti-idiotypic Fab complex, *Proc. Natl. Acad. Sci.* 91 (5) (1994) 1604–1608.
- [25] D. Issadore, et al., Miniature magnetic resonance system for point-of-care diagnostics, *Lab Chip* 11 (2011) 2282–2287.
- [26] H. Lee, et al., Chip-NMR biosensor for detection and molecular analysis of cells, *Nat. Med.* 14 (2008) 869–874.
- [27] I. Koh, et al., Nanoparticle-target interactions parallel antibody-protein interactions, *Anal. Chem.* 81 (2009) 3618–3622.